AADE-23-NTCE-063

Non-Newtonian Clogged Flows in Bifurcated Pipelines and Conduits

Jamie A. Chin and Michael C. McKinley, Stratamagnetic Software, LLC

Abstract

Fluid flows in pipeline systems are ubiquitous to drilling and cementing operations. Many models relating pressure gradient to flow rate are available for different rheologies, the best known being Hagen-Poiseuille's law for Newtonian liquids in circular conduits. However, real flows seldom follow ideal constitutive relations, and more often than not, are plugged by unpredictable, asymmetric distributions of wax, hydrates or debris. In "Non-Newtonian Flow in Clogged Non-Circular Piping Conduits," AADE-22-FTCE-006, we modeled non-Newtonian flow for standard rheologies in conduits having arbitrary cross-section to accommodate blockages with general geometries. When a flow domain is described by user-defined coordinates, a custom curvilinear grid is created for that geometry, allowing no-slip conditions to be accurately applied along all wall and blockage boundaries. Calculated results for different blockage shapes, exact in the foregoing sense, were presented for different fluid models and clogs.

This methodology is extended to handle systems of connected or bifurcated pipes, in the general case, having the appearance of a river branching into multiple tributaries, with each flow unfolding into still more branches. The algorithm is first developed for Newtonian, Power Law, Bingham Plastic and Herschel-Bulkley liquids in *circular* pipes, and then, in detail for Newtonian flows in *clogged* pipes (non-Newtonian extensions are given). We show how the earlier single-element clogged pipe model can be combined with the bifurcation model to simulate flow in clogged piping systems. Unlike simulations using numerically intensive finite element solvers, requiring specialized hardware and software licenses, the present approach, portable and analytically based, reveals fundamental physical trends identified with explicit input parameters, requiring only the solution of nonlinear algebraic equations describing junction pressures at pipe intersections.

1. Clogged Pipe Overview

Computational fluid dynamics, or "CFD modeling," uses advanced numerical techniques to solve partial differential equations rapidly and accurately for engineering applications. Perhaps the greatest impediment to progress is not so much formal algorithm design, for example, finite difference versus finite element implementations, but more so the mundane application of boundary constraints that describe the problem at hand. Often these are obvious. For example, circular pipe cross-sections require polar coordinates, while flows in rectangular air conditioning ducts are more amenable to solutions in Cartesian coordinates. For both of these problems, exact analytical solutions are available in the literature which have proven useful in countless applications.

The boundary conditions for clogged pipe flows in general bifurcated systems are dual in nature. At the local scale, zero slip velocity constraints apply at solid surfaces, which include pipe walls and general debris interfaces. At the global macroscopic level, the topology of the branched piping system controls the overall flow. The manner in which large-scale constraints are applied affects the physical integrity of the entire solution. For example, viscous wall shear stresses, which affect erosion, are affected, as are global flow rate versus pressure gradient relations. An "isolated clog" affects flow in its own pipe element and more – it invariably affects flows in all system branches, and all local effects depend on interactions between inlet and outlet pressures everywhere.

Figure 1-1. Real world asymmetric clog blockages.

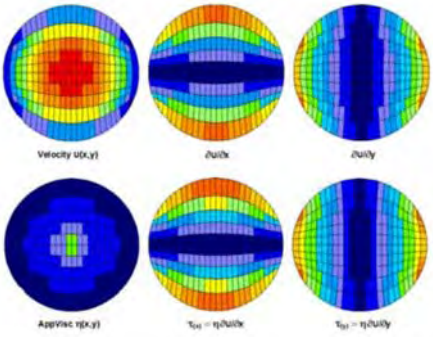

Figure 1-2. Boundary-conforming, curvilinear grids with small internal *rectangular* area elements.

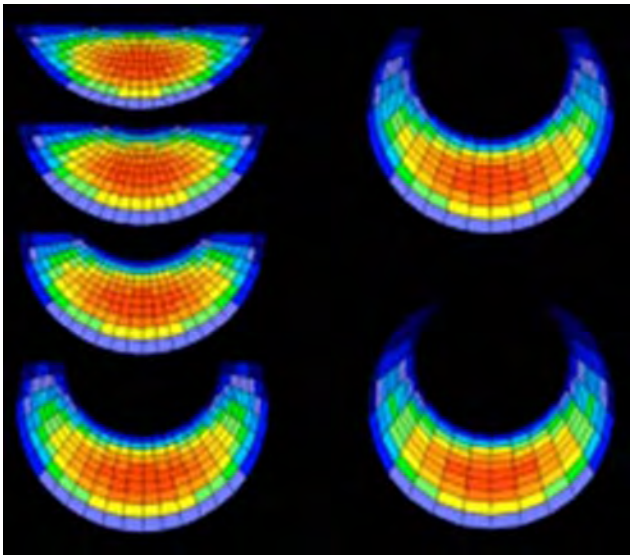

Figure 1-3. "Smile like" flow domains.

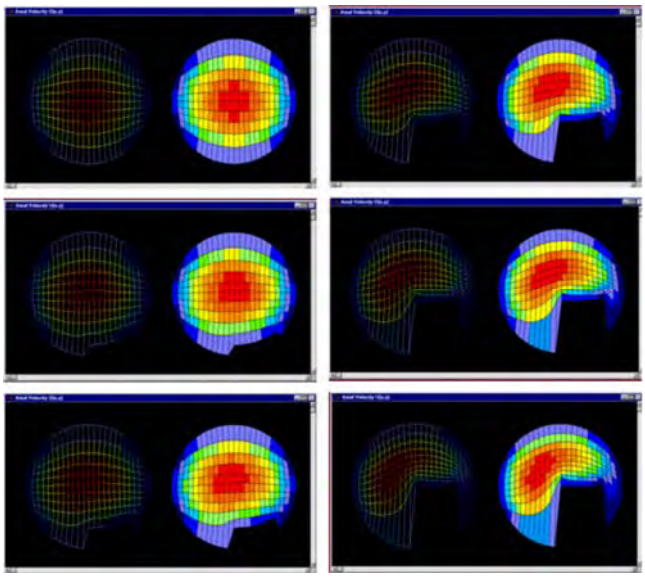

Figure 1-4. Lumped blockages growing in time.

The first problem of single-element pipe flow with clogs of arbitrary cross-sectional shape has been solved recently (Chin 2022). Recognizing that circular pipes are often affected by "upper and lower" anomalies like floating wax deposition and bottom debris segregation driven by gravity, and "left and right" geometric displacement changes responding to mass conservation requirements, the earlier work introduced *internal* rectangular-like "boundary conforming, curvilinear" grids that apply no-slip conditions at pipe walls in the usual manner while adapting to foregoing "up, down, left and right" requirements in the flow domain.

The grid generation method is discussed in the 2022 paper. It is important to summarize this new technology here since it plays an integral role in the broader bifurcation problem. Figure 1-1 illustrates real-world clog blockages defining the focus of our work. The top left of Figure 1-2 shows the velocity distribution in a circular pipe, where red indicates high speeds in the central core while blue represents low speeds near the wall. Closer examination shows that polar coordinates defined by concentric circles and radial lines are *not* used. In fact, the area elements in the curved grid domain are *rectangular* in the vertical x and horizontal y directions.

The middle upper and lower shear rate $\partial U/\partial x$ and viscous stress $\eta(x,y)$ $\partial U/\partial x$) distributions show bright zones at the top and bottom, making these components natural candidates for debris growth or wax removal analysis (note $U(x,y)$ and $\eta(x,y)$ are axial speed and apparent viscosity). This is so because the component of strain that varies with the vertical x is the one that controls anomaly growth at upper and locations. Similar considerations apply to the horizontal directions y at the far right column. The bottom left displays calculated apparent viscosities found in non-Newtonian flows that vary throughout the cross-sectional geometry. Finally, Figures 1-3 and 1-4 show computed velocities for different classes of clogs; for programming convenience, colors represent different speeds from one example to another, e.g., all reds are not equal in magnitude. In summary, the 2022 work, using new ideas in grid generation, supported accurate predictions for flow rate versus pressure gradient behavior and viscous stress for arbitrary cross-sectional geometries and general rheologies.

2. Newtonian Bifurcated Flow Overview

The prior work was simple in that the underlying model was two-dimensional, meaning that variations in a third axial direction "z" were not considered. At this point, two natural questions arose. First, how are clog non-uniformities along z handled? This problem is easily addressed numerically. Suppose we have a conduit whose cross-sectional geometry varies with z, while containing a general clog whose geometry also changes in the z direction. We would then discretize the pipe into elementary Δz lengths and solve for the flow in each elemental component, assuming the same volume flow rate, for the pressure drop ΔP describing that element. Then, the total system pressure drop is obtained by summing all the ΔPs while the local pressure gradients are available from known $\Delta P/\Delta z$ values. These might be useful for studies related to flow separation or other inefficiencies. We will not discuss this axial flow problem further in the paper.

The second problem is more challenging. Certainly, many undergraduate students of engineering have "solved" the problem of ideal flow through a conduit that bifurcates into multiple branches in homework exercises. The usual approach, which assumes total energy conservation and conveniently leads to closed form solutions, is well known and offered in tutorial websites such as www.chegg.com. However, the method and results are misleading because friction is not accounted for, and incorrect as fluid movements cannot be sustained in reality without energy or power addition.

For this reason, piping designs are often pursued empirically, using laboratory determined head loss or friction factors that vary with surface finish, inlet distance, anomalies at pipe connections, and so on. A major limitation is their

failure in modeling fluid rheology effects, despite the fact that single pipe formulas analogous to the Hagen-Poiseuille law for Newtonian flow have been available for over a century. In this paper, we will develop an analytically based method for flows in bifurcated piping systems that incorporates classic pipe flow results at the local level. At the global level, in our treatment of branched systems, we will not assume total energy conservation, which is unrealistic physically. Instead, we require that total mass is conserved, which is reasonable. This leads to anticipated losses in momentum and energy associated with wall stresses. We further show how an earlier clogged pipe model (Chin 2022) can be used within the framework of the bifurcation model. The complete analytical derivations are given for a Newtonian fluid, and extensions to Power Law, Bingham Plastic and Herschel-Bulkley fluids are also presented. Example calculations are given, and in particular, we demonstrate how the model can be used to solve for branched flows containing clog distributions such as those shown in Figures 1-3 and 1-4.

2.1 Newtonian flow in simple bifurcations

We will present detailed discussions, including all math derivations for bifurcated flow properties, for Newtonian fluid motions first. This is initially pursued for pipes that expand into only two sections, and then, into more general networks. All results are presented in terms of closed form, analytical expressions. Following this presentation, we consider nonlinear rheologies such as Power Law, Bingham Plastic and Herschel-Bulkley models, which in part rely on numerically based algorithms. In the final section of this paper, example calculations are given for single-element pipes and we also demonstrate how their results can be incorporated into those for branched pipelines with clogged cross-sections.

We start with Hagen-Poiseuille's classic law for the volume flow rate "$Q = \pi R^4(P_i - P_o)/(8\mu L)$." The assumptions: (a) circular cross-section of radius R, (b) a straight conduit with length L satisfying L >> R, (c) a liquid viscosity of μ, (d) end pressure conditions with P_i and P_o respectively being inlet and outlet values, (e) steady-state laminar flow, (f) smooth walls and (g) a location away from inlets. We will assume that $Q > 0$ if $P_i > P_o$. Fluid density does not appear in Hagen-Poiseuille's law because steady-state conditions are assumed; density, however, is important in transient applications.

Consider the uneven bifurcation in Figure 2-1, where the main flow rate Q_1 in "1" feeds into branches "2" and "3" as shown at the top. For constant density flow, mass conservation requires that $Q_1 = Q_2 + Q_3$. Here mass considerations disallow momentum and energy conservation, both of which are not possible when irreversible viscous wall losses are present. Applying the rule to each pipe flow segment directly produces $Q_1 = \pi R_2^4 (P_a - P_{o,2})/(8\mu L_2) + \pi R_3^4 (P_a - P_{o,3})/(8\mu L_3)$. Here, $P_{o,2}$ and $P_{o,3}$ are branch "2" and "3" outlet pressures, while at the junction "*a*," we determine the pressure as

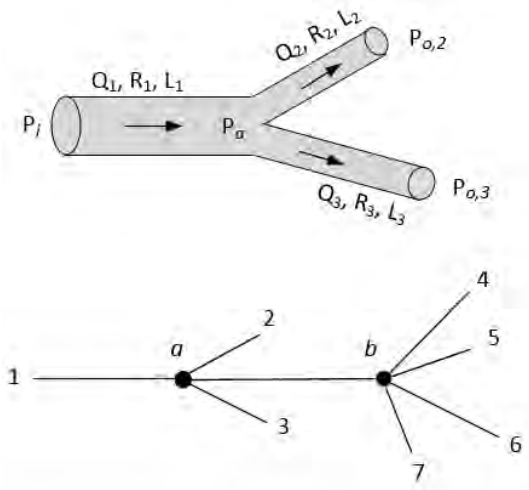

Figure 2-1. Two-branch bifurcation (top), with multi-branch geometry (bottom).

$$P_a = \{8\mu Q_1/\pi + (R_2^4 P_{o,2}/L_2 + R_3^4 P_{o,3}/L_3)\}/ \{R_2^4/L_2 + R_3^4/L_3\} \quad (2.1)$$

This can be introduced into the rate formulas

$$Q_2 = \pi R_2^4 (P_a - P_{o,2})/(8\mu L_2) \quad (2.2)$$

$$Q_3 = \pi R_3^4 (P_a - P_{o,3})/(8\mu L_3) \quad (2.3)$$

to give the flow rates Q_2 and Q_3 into branches "2" and "3."

We could also have expressed "$Q_1 = Q_2 + Q_3$" in the form $R_1^4 (P_i - P_a)/L_1 = R_2^4 (P_a - P_{o,2})/L_2 + R_3^4 (P_a - P_{o,3})/L_3$ to show $P_a = (R_1^4 P_i/L_1 + R_2^4 P_{o,2}/L_2 + R_3^4 P_{o,3}/L_3)/(R_1^4/L_1 + R_2^4/L_2 + R_3^4/L_3)$. Introduce this in $Q_1 = \pi R_1^4 (P_i - P_a)/(8\mu L_1)$ and we find that

$$Q_1 = \{\pi R_1^4/(8\mu L_1)\} \times [P_i - \{(R_1^4 P_i/L_1 + R_2^4 P_{o,2}/L_2 + R_3^4 P_{o,3}/L_3)/(R_1^4/L_1 + R_2^4/L_2 + R_3^4/L_3)\}] \quad (2.4)$$

which can be solved for inlet pressure as follows

$$P_i = Q_1 + \{\pi R_1^4/(8\mu L_1)\}\ \{(R_2^4 P_{o,2}/L_2 + R_3^4 P_{o,3}/L_3)/(R_1^4/L_1 + R_2^4/L_2 + R_3^4/L_3)\} \quad (2.5)$$

$$\{\pi R_1^4/(8\mu L_1)\} - \{\pi R_1^8/(8\mu L_1^2)\}/(R_1^4/L_1 + R_2^4/L_2 + R_3^4/L_3)$$

Finally, the viscous shear stresses τ acting at the walls of branches "1," "2" and "3" are given by

$$\tau_1 = (P_i - P_a)\ R_1/(2L_1) \quad (2.6)$$

$$\tau_2 = (P_a - P_{o,2})\ R_2/(2L_2) \quad (2.7)$$

$$\tau_3 = (P_a - P_{o,3})\ R_3/(2L_3) \quad (2.8)$$

which follow from global momentum balances. These equations all solve different flow problems.

Case 1. Flow rate Q_1 prescribed. If the main flow rate Q_1 is prescribed, together with the outlet pressures $P_{o,2}$ and $P_{o,3}$, and if all lengths, radii, and viscosity are given, then the volume flow rates in branches "2" and "3" are determined by Equations 2.2 and 2.3 where the junction pressure P_a is defined by Equation 2.1. The inlet pressure where the main flow enters is calculated from Equation 2.5. This formulation addresses the following problems. When pumping operations are in progress, will the inlet pressure P_i exceed a pre-defined "burst pressure" and lead to breakage? Will the rates Q_2 and Q_3 be rapid enough to deliver needed flows to subsidiary pipe elements? Will viscous shears be so excessive so as to induce wear and tear or increase power requirements? How might R and L be altered to achieve operational targets? In health care, options may include increases in R (through clog removal and stent usage), decreases in L (as in a shortening of varicose veins), or reductions in viscosity using blood thinners.

Case 2. Inlet pressure P_i prescribed. If the inlet pressure is prescribed, together with the outlet pressures $P_{o,2}$ and $P_{o,3}$, and if all lengths, radii and viscosity are given, then the main flow rate Q_1 is known from Equation 2.4. This can be substituted in Equation 2.1 to give the junction pressure P_a, which is in turn used in Equations 2.2 and 2.3 to provide Q_2 and Q_3. We might similarly ask, "Is Q_1 rapid enough to deliver needed flows to all piping elements?" For the geometries assumed, will Q_2 and Q_3 meet flow requirements? How can the junction pressure P_a be increased to improve these flow rates? Can we alter R_2 and L_2 to effect changes in branch "3" if this branch itself is not easily accessible?

Case 3. Identical outlet pressures $P_{o,2}$ and $P_{o,3}$ are given. In this case, we write $P_{o,2} = P_{o,3} = P_o$. Here, the geometries for branches "2" and "3" may differ. For instance, one conduit may be longer than the other, with both having different radii – however, we assume that their outlets are sufficiently close in proximity so that their exit pressures will also be close. In other applications, the two may be geometrically identical but situated far apart – an obvious example in healthcare is found in the left and right iliac arteries that transport blood through the pelvis and legs. Then, Equation 2.1 simplifies considerably and introducing this into Equations 2.2 and 2.3 shows that

$$P_a = P_o + (8\mu Q_1/\pi)/(R_2^4/L_2 + R_3^4/L_3) \quad (2.9)$$

$$Q_2 = (Q_1 R_2^4/L_2)/(R_2^4/L_2 + R_3^4/L_3) \quad (2.10)$$

$$Q_3 = (Q_1 R_3^4/L_3)/(R_2^4/L_2 + R_3^4/L_3) \quad (2.11)$$

These results are interesting. First, Q_2 and Q_1 are related only by a simple geometric factor $(R_2^4/L_2)/(R_2^4/L_2 + R_3^4/L_3)$ that is independent of viscosity and pressure – this similarly applies to Q_3 and Q_1. Second, the quantity " $Q_2 + Q_3$" can be evaluated from Equations 2.10 and 2.11 to demonstrate that $Q_2 + Q_3 = Q_1$, which states that mass is conserved as assumed.

And third, a simple "energy like" law follows from Equations 2.10 and 2.11. Squaring these leads to $Q_2^2 = (Q_1^2 R_2^8/L_2^2)/(R_2^4/L_2 + R_3^4/L_3)^2$ and $Q_3^2 = (Q_1^2 R_3^8/L_3^2)/(R_2^4/L_2 + R_3^4/L_3)^2$. Adding the two gives

$$\begin{aligned} Q_2^2 + Q_3^2 &= Q_1^2 (R_2^8/L_2^2 + R_3^8/L_3^2)/(R_2^4/L_2 + R_3^4/L_3)^2 \\ &= Q_1^2 \{(R_2^8/L_2^2 + R_3^8/L_3^2)/(R_2^8/L_2^2 + 2R_2^4 R_3^4/L_2L_3 + R_3^8/L_3^2)\} \end{aligned} \quad (2.12a)$$

This as an energy-equation for energy dissipated in the bifurcation process, with { } being the loss factor. Since { } is a fraction less than one, with its denominator exceeding the numerator, we have the inequality

$$Q_2^2 + Q_3^2 < Q_1^2 \quad (2.12b)$$

Thus, while the mass conservation in $Q_2 + Q_3 = Q_1$ holds, the sum of the squares in volume flow rates, a quantity related to kinetic energy, is not conserved. By contrast, it must follow Equation 2.12b for the Newtonian model assumed. The above equations are useful for quick "back of the envelope" calculations. In closing, mass conservation using $Q_2 + Q_3 = Q_1$ allows an abrupt lossy transition from a single conduit to a doubly-bifurcated system (local flow reversals are not described). In reality, fluid-dynamical motions can be very complicated at such junctions, but these will require lengthy and detailed three-dimensional finite element analyses.

2.2 Software – CODE-1 for two uneven bifurcated arteries with Q_1 specified.

The above results are easily programmed using spreadsheet methods, but they are more conveniently accessible in the CODE-1 utility of Figure 2-2 developed originally for healthcare problems. A symmetric artery system is shown, as for the left and right iliac arteries discussed earlier, but we emphasize that the model applies to systems without symmetry as in most engineering problems.

An initial calculation. To validate our bifurcated flow programming, assume that branches "1," "2" and "3" are geometrically identical. In Figure 2-2, white text boxes are reserved for data inputs, while non-editable gray boxes are intended for displays of calculated quantities. Clicking "Find" in Figure 2-3 conveniently computes all of the flow attributes. The program correctly shows that the assumed flow rate of "100 cc/s" splits into two identical flows of 50 cc/s each. The pressure drops in branches "2" and "3" are 2.00373 – 2 = 0.00373 psi, while that in "1" is 2.01119 – 2.00373 = 0.00746 psi. This is exactly twice "0.00373 psi" and is consistent with a flow rate ratio of two to one, obtained on comparing 100 to 50 cc/s. This linear dependence of volume flow rate on pressure drop is a property of Newtonian fluids. Here we note that the Newtonian assumption is only applicable to larger diameter blood vessels. The identical results obtained for branches "2" and "3" validate the complicated equations, computer programming logic and units conversion facilities.

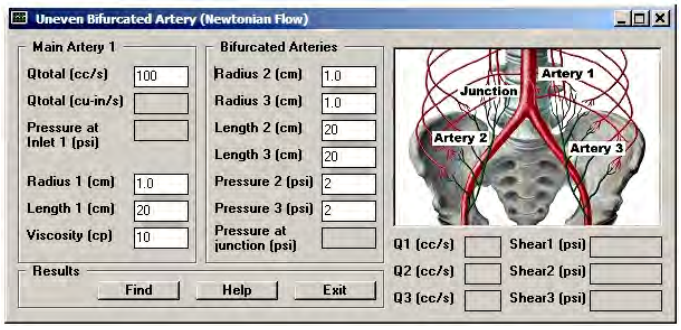

Figure 2-2. Forward model with Q_1 given (Ref. CODE-1).

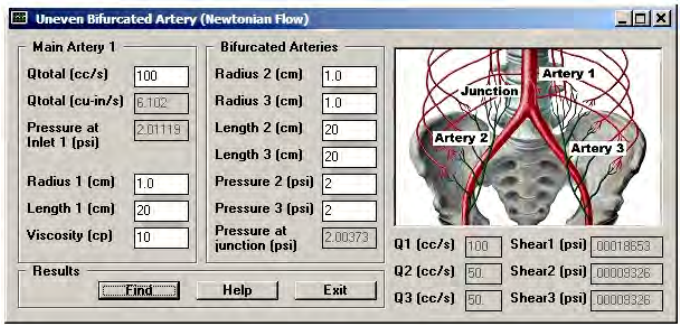

Figure 2-3. Calculated results appear in gray boxes (symmetical bifurcation data are used to validate computed results for required symmetric solutions).

A second calculation. Now let us consider for purposes of validation the example in Figure 2-4. Here the branches in "2" and "3" are again identical, but longer and narrower than that in "1." The pressure drop in "1" is now 2.12684 – 2.11938 = 0.00746 psi, while those in "2" and "3" are 2.11938 – 2 = 0.11938 psi. Even though the flow rate in "1" is twice that of "2" or "3," the pressure drop is much smaller, because the radius in "1" is twice as large. The total pressure drop from inlet to outlet is 2.12684 – 2 = 0.12684 psi. Another Newtonian flow property is worth mentioning. If the viscosity is halved to 5 psi, the total pressure drop becomes 2.06342 – 2 = 0.06342 psi, which is half of 0.12684 psi (software screen not shown). In other words, a decrease in viscosity leads to a proportional decrease in pressure drop. This "scalability" does not apply to non-Newtonian fluids, which are treated later.

We emphasize that a given applications problem may require different rheological models at different locations within the flow. For example, in healthcare, a wide body of literature supported by empirical laboratory data shows that blood flows in the larger main aorta blood vessel satisfy Newtonian models, while those in smaller diameter downstream vessels require non-Newtonian models. Difficulties in modeling arise when different piping elements require different "n" and "K" parameter inputs.

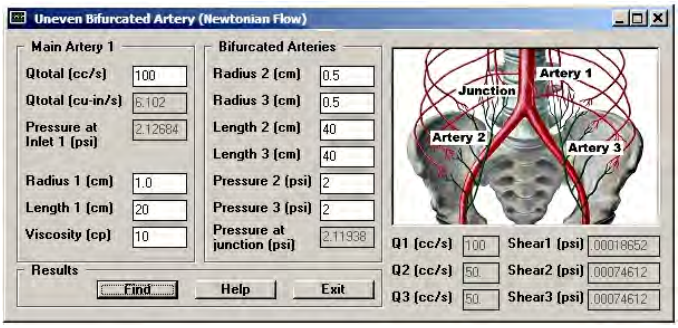

Figure 2-4. Branch "1" different from identical "2" and "3."

2.3 Theory – Two uneven bifurcated arteries with P_i specified

The above applies when Q_1 is the main input. Earlier we showed how if P_i, $P_{o,2}$ and $P_{o,3}$ are known, the junction pressure is $P_a = (R_1^4 P_i/L_1 + R_2^4 P_{o,2}/L_2 + R_3^4 P_{o,3}/L_3)/(R_1^4/L_1 + R_2^4/L_2 + R_3^4/L_3)$. Then, the inlet flow rate is $Q_1 = \pi R_2^4 (P_a - P_{o,2})/(8\mu L_2) + \pi R_3^4 (P_a - P_{o,3})/(8\mu L_3)$. With these quantities available, an analysis similar to the above is straightforward.

2.4 Software – CODE-2 for two uneven bifurcated arteries with P_i specified

We now describe the software "CODE-2" where P_i is given. Obviously, CODE-1 and CODE-2 are complementary. They were developed separately to keep the programming logic simple. Figure 2-5 shows both side-by-side and creates consistent numerical outputs to four decimal places.

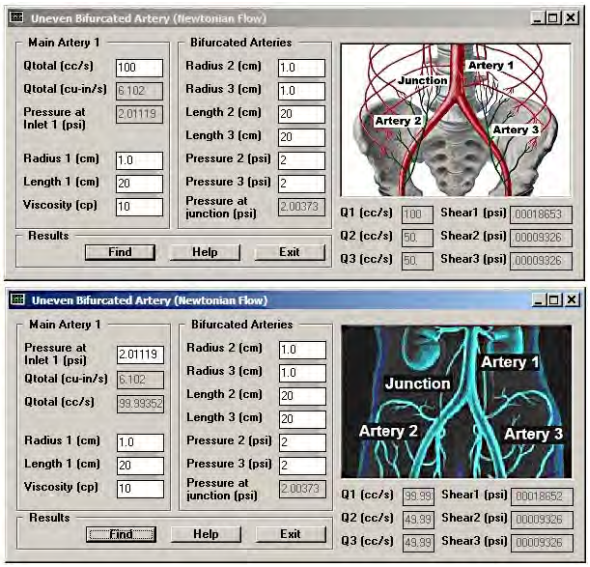

Figure 2-5. Complementary CODE-1 and CODE-2 implementations.

2.5 Theory – Complicated network flows with chained bifurcations

Now let us study a more complicated network with additional bifurcations, as shown in Figure 2-6. It is not the most general, nor was it intended to be. We wish only to demonstrate the mathematical manipulations needed to handle networks of greater complexity, so researchers can develop customized models as needed. For clarity, we omit all "outlet" subscripts, e.g., $P_{o,2}$ becomes P_2.

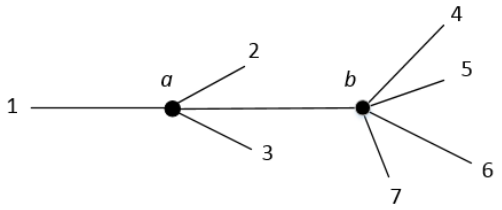

Figure 2-6. A more complicated flow network.

As before, we start with Hagen-Poiseuille's law, as given in Equations 2.13 and 2.14. The parameter "A" is introduced for simplicity, to eliminate an error-prone "$\pi/(8\mu)$." Whereas we chose "$Q_1 = Q_2 + Q_3$" before, we now perform the operation twice, as in Equations 2.15 and 2.16 – that is, once for each network, focusing on the junctions *a* and *b*.

$$Q = \pi R^4(P_i - P_o)/(8\mu L) \tag{2.13}$$

$$Q = AR^4(P_i - P_o)/L \text{ where } A = \pi/(8\mu) \tag{2.14}$$

$$Q_{1a} = Q_{a2} + Q_{a3} + Q_{ab} \tag{2.15}$$

$$Q_{ab} = Q_{b4} + Q_{b5} + Q_{b6} + Q_{b7} \tag{2.16}$$

We next introduce Equation 2.14 into the *right side* of Equation 2.15, and Equation 2.14 into *all terms* in Equation 2.16. This leads to

$$\begin{aligned} Q_{1a} &= AR_{a2}^4(P_a - P_2)/L_{a2} \\ &\quad + AR_{a3}^4(P_a - P_3)/L_{a3} + AR_{ab}^4(P_a - P_b)/L_{ab} \end{aligned} \tag{2.17}$$

$$\begin{aligned} R_{ab}^4(P_a - P_b)/L_{ab} &= R_{b4}^4(P_b - P_4)/L_{b4} + R_{b5}^4(P_b - P_5)/L_{b5} \\ &\quad + R_{b6}^4(P_b - P_6)/L_{b6} + R_{b7}^4(P_b - P_7)/L_{b7} \end{aligned} \tag{2.18}$$

The above can be re-expressed as "two equations for two unknowns" in the algebraic sense. The unknowns are the junction pressures P_a and P_b, as indicated in Equations 2.19 and 2.20, with coefficients **B**, **C**, **D**, **E**, **F** and **G** as in Equations 2.24 – 2.26. The solutions appear in Equations 2.27 and 2.28.

$$\mathbf{B}P_a + \mathbf{C}P_b = \mathbf{D} \tag{2.19}$$

$$\mathbf{E}P_a + \mathbf{F}P_b = \mathbf{G} \tag{2.20}$$

$$\mathbf{B} = A(R_{a2}^4/L_{a2} + R_{a3}^4/L_{a3} + R_{ab}^4/L_{ab}) \tag{2.21}$$

$$\mathbf{C} = -A\,R_{ab}^4/L_{ab} \tag{2.22}$$

$$\mathbf{D} = Q_{1a} + AR_{a2}^4P_2/L_{a2} + AR_{a3}^4P_3/L_{a3} \tag{2.23}$$

$$\mathbf{E} = R_{ab}^4/L_{ab} \tag{2.24}$$

$$\mathbf{F} = -(R_{ab}^4/L_{ab} + R_{b4}^4/L_{b4} + R_{b5}^4/L_{b5} + R_{b6}^4/L_{b6} + R_{b7}^4/L_{b7})$$

$$\mathbf{G} = -(R_{b4}^4P_4/L_{b4} + R_{b5}^4P_5/L_{b5} + R_{b6}^4P_6/L_{b6} + R_{b7}^4P_7/L_{b7}) \tag{2.25, 2.26}$$

$$P_a = (\mathbf{DF} - \mathbf{CG})/(\mathbf{BF} - \mathbf{CE}) \tag{2.27}$$

$$P_b = (\mathbf{BG} - \mathbf{DE})/(\mathbf{BF} - \mathbf{CE}) \tag{2.28}$$

The final steps involve post-processing for inlet pressure, flow rates and shear stresses. First, from Equation 2.14, the relationship "$Q = AR^4(P_i - P_o)/L$" suggests that we can write $Q_1 = AR_1^4(P_i - P_a)/L_1$. Since Q_1 is prescribed and P_a is known from above, this yields

$$P_i = P_a + Q_1L_1/(AR_1^4) \tag{2.29}$$

It suffices to consider a typical branch from each of junctions "*a*" and "*b*." For example, from "*a*," we have

$$Q_2 = AR_2^4(P_a - P_2)/L_2 \tag{2.30}$$

$$\tau_2 = (P_a - P_2)R_2/(2L_2) \tag{2.31}$$

while from "*b*," we have

$$Q_6 = AR_6^4(P_b - P_6)/L_6 \tag{2.32}$$

$$\tau_6 = (P_b - P_6)R_6/(2L_6) \tag{2.33}$$

Software can be readily developed from the above for Figure 2-6 and similar networks. We leave this to the interested reader.

2.6 Network with arbitrary number of bifurcations

Now let us consider an earlier problem where Q_1 is given, and the junction pressure P_a and inlet pressure P_i are required, but now an arbitrary number of bifurcations (having different radii and lengths) with n = 2, 3, 4 . . . N being allowed. Volume flow rates and shear stresses in all sub-branches will be derived. The most popular application will probably be the two-branch model whose solution was already worked out in detail. However, the present generalization will be useful for predictions in more complicated networks.

We begin by expressing mass conservation law $Q_1 = Q_2 + Q_3 + \ldots + Q_N$ in summation notation, where the sum Σ is taken over the indexes n = 2, 3, 4 . . . N, that is,

$$Q_1 = \{\pi/(8\mu)\}\,\Sigma\,R_n^4(P_a - P_n)/L_n \tag{2.34}$$

The constant P_a can be factored out and solved as

$$P_a = (8\mu Q_1/\pi + \Sigma\,R_n^4P_n/L_n)/\Sigma(R_n^4/L_n) \tag{2.35}$$

If we rewrite Equation 2.34 in the expanded format as $R_1^4(P_i - P_a)/L_1 = \Sigma\,R_n^4(P_a - P_n)/L_n$, the inlet pressure is

$$P_i = P_a[1 + (L_1/R_1^4)\Sigma\,R_n^4/L_n] - (L_1/R_1^4)\Sigma\,R_n^4P_n/L_n \tag{2.36}$$

where the P_a on the right side is known from Equation 2.35. Then, the flow rates and viscous shear stresses below are obtained.

$$Q_n = \pi R_n^4 (P_a - P_n) /(8\mu L_n) \quad (2.37)$$

$$\tau_1 = (P_i - P_a) R_1 /(2 L_1) \quad (2.38)$$

$$\tau_n = (P_a - P_n) R_n /(2 L_n) \quad (2.39)$$

Extensions to networks more complicated than shown in Figure 2-6 are straightforward. The "summation strategy" above would apply to a sequence "*a*, *b*, *c*, *d* . . ." of junction point problems, and coupled linear algebraic equations for P_a, P_b, P_c, P_d and so on, would be solved. Then, the inlet pressure is derived, followed by results for all branch volume flow rates and viscous shear stresses.

3. Non-Newtonian Bifurcated Flow Overview

In this section, we consider non-Newtonian flows in circular conduits and networks formed from such sections. Because nonlinear relations connect flow rates to pressure differentials, simple analytical solutions are not possible and recourse is made to numerical methods. We first illustrate our approach for the simplest "Power Law" model. Then, corresponding models are developed for Bingham Plastic and Herschel-Bulkley and detailed explanations are offered.

3.1 Power Law Fluids

In the simplest case, the viscous shear stress τ and the axial velocity profile U(r) are related by $\tau(r) = k \{dU/dr\}^n$ where r is the radial coordinate, "n" is a dimensionless exponent and "k" is the "consistency index." This leads to the well known volume flow rate relationship

$$Q = \{n\pi R^3/(3n + 1)\} [R(P_i - P_o)/(2kL)]^{1/n} \quad (3.1)$$

The Newtonian Hagen-Poiseuille law is obtained by setting n = 1 and the consistency factor to $k = \mu$, where μ is the constant viscosity, leading to $Q = \pi R^4(P_i - P_o)/(8\,\mu\, L)$. The assumptions for the Power Law model are similar. They are: (a) a circular cross-section of radius R, (b) a straight conduit with length L satisfying L >> R, (c) constant values of k and n, (d) end conditions with P_i and P_o being inlet and outlet pressures, and (e) steady-state flow. The convention used assumes that the flow rate Q > 0 if $P_i > P_o$. Note that fluid density does not appear because steady-state, laminar (non-turbulent) conditions are assumed – density, however, will appear in transient and compressible flow applications.

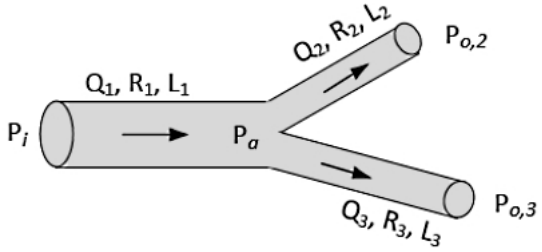

Figure 3-1. Simple two-branch bifurcation.

We consider the two-branch bifurcation in Figure 3-1. Conservation of mass requires that $Q_1 = Q_2 + Q_3$ where Q_1 is specified so that we may write

$$Q_1 = \{n\pi R_2^3/(3n + 1)\} [R_2(P_a - P_{o,2})/(2kL_2)]^{1/n} + \{n\pi R_3^3/(3n + 1)\} [R_3(P_a - P_{o,3})/(2kL_3)]^{1/n} \quad (3.2)$$

Iterative "half-step" solution for P_a and P_i. Earlier, we solved for the junction pressure P_a first, and using it, derived expressions for Q_2 and Q_3. The algebra was simple although lengthy manipulations were necessary. However, in this problem, "n" is general, possibly taking on integer and fractional values, so that an expression for P_a could not be obtained. In fact, Equation 3.2 is nonlinear. One might attempt to use Newton-Raphson schemes popular in solving nonlinear polynomial equations, but these converge slowly and rely on the availability of initially close solutions. The method below is robust and yields solutions with minimal user interaction, while furthermore applying to more complicated rheological models considered later for our problems.

When Q_1, $P_{o,2}$ and $P_{o,3}$ are given, we would expect Q_1 to monotonically increase as P_a increases. This behavior can be used to derive the required solution. We start with a guess, the best being the *greater* of $P_{o,2}$ and $P_{o,3}$, to ensure that the quantities in the square brackets of Equation 3.2 are both positive. Then, as P_a is successively increased by given ΔP increments, the right hand side "RHS" of Equation 3.2 will increase until the ratio "$RHS/Q_{1,prescribed}$" exceeds unity. This means that we have over-predicted both P_a and Q_1. To compensate for this, we return to our "previous P_a" and guess using a reduced $\Delta P/2$. If we still over-predict, the iterative process is repeated, with this recursive "half step" operation continued until a specified error bound is satisfied.

Once we have obtained P_a, we turn to Equation 3.1 to infer the algebraic form for volume flow rate expressions in "1" and the two downstream branches "2" and "3." This allows us to write the solutions

$$Q_1 = \{n\pi R_1^3/(3n + 1)\} [R_1 (P_i - P_a) /(2kL_1)]^{1/n} \quad (3.3)$$

$$Q_2 = \{n\pi R_2^3/(3n + 1)\} [R_2 (P_a - P_{o,2})/(2kL_2)]^{1/n} \quad (3.4)$$

$$Q_3 = \{n\pi R_3^3/(3n + 1)\} [R_3 (P_a - P_{o,3})/(2kL_3)]^{1/n} \quad (3.5)$$

Equation 3.3 can be solved to produce the inlet pressure P_i for branch "1," with the result that

$$P_i = P_a + (2kL_1/R_1) [(3n+1) Q_1/(n\pi R_1^3)]^n \quad (3.6)$$

Shear stress. For Power Law pipe flows, known results for laminar viscous shear stress can be used. For such problems, $\tau = k (- dU/dr)^n$ where the velocity profile satisfies $U(r) = ((P_i - P_a)/(2kL_1))^{1/n} [n/(n+1)] (R_1^{(n+1)/n} - r^{(n+1)/n})$. This leads to $(- dU/dr)^n = ((P_i - P_a)/(2kL_1))\, r$, which in turn yields the formula $\tau = k(- dU/dr)^n = (P_i - P_a) R_1/(2L_1) > 0$ at $r = R_1$. Similar results are obtained at R_2 and R_3, so that,

$$\tau_1 = (P_i - P_a) \quad R_1/(2L_1) \tag{3.7}$$

$$\tau_2 = (P_a - P_{o,2})\, R_2/(2L_2) \tag{3.8}$$

$$\tau_3 = (P_a - P_{o,3})\, R_3/(2L_3) \tag{3.9}$$

These results are identical to those for Newtonian fluids as they follow from global considerations that balance pressure force and wall shear effects. For complicated geometries containing general clogs, the details of the clog and fluid interface enter and these formulas do not apply. This is studied earlier (Chin 2022; Chin and Chin, 2022).

Typical parameters. The earlier solution for P_a can be written in Fortran as in Figure 3-2. Five examples are provided below. The physical units LBF, IN and SEC for pound force, inch and second are used. Pressure is then represented by PSI or LBF/IN^2. For water at room temperature and pressure, the Newtonian inputs are n = 1 and k = μ = 0.0000001465 psi sec. Examples for blood flow applications appeared earlier (Chin and Chin, 2022). We use their assumptions – a consistency index of k = 17.0 mPa sec ^{n} for healthy control subjects. In our physical units, this is 17 (0.0000001450 psi sec ^{n}) or 0.000002465 psi sec ^{n} – a bit less than 17 cp, *if* n were equal to unity. They also found n values slightly greater than 0.7, supporting their observation that blood mixtures are Power Law fluids. Others have assumed 10 – 15 cp viscosities range, with similar findings for n. To assess the robustness of our algorithms, we considered high and low sides of n and k values. Note that Power Law models neglect yield stresses. When these are important, the Power Law model becomes a Herschel-Bulkley fluid, which will be considered later. We next turn to the algorithm BIFURC-4 for junction pressure P_a, shown in its entirety in Figure 3-2.

```
C      BIFURC-4.FOR (Power Law Model, Simple Network)

       REAL K,L1,L2,L3

       CHARACTER*1 REPLY
       PI = 3.1415926
C
C      Physical units used - LBF, IN, SEC, PSI
C
C      For Newtonian water flows of 1 cp, the power law
parameters
C      are EN = 1.0 and K = 0.0000001465 -  the constant
Newtonian
C      viscosity VISC is not used.  To study water with 10
cp, use
C      EN = 1.0, K = 10.*0.0000001465, NMAX = 500, DP =
0.00001 to
C      find junction pressure PA solutions.  NMAX and DP are
found
C      by trial and error.  The solution is obtained when
test and
C      assumed flow rates are identical, that is, having
RATIO = 1.
C
C      Inputs ...
C
            WRITE(*,5)
       5    FORMAT(1X,'Example 1-5?  Enter:  ',$)
            READ(*,6) NCASE
       6    FORMAT(I1)
            IF(NCASE.EQ.1) GO TO 10
            IF(NCASE.EQ.2) GO TO 12
            IF(NCASE.EQ.3) GO TO 14
            IF(NCASE.EQ.4) GO TO 16
            IF(NCASE.EQ.5) GO TO 18
C      Example 1 (10 cp Newtonian)
        10  EN = 1.0
            K = 10.*0.0000001465
            DP = 0.00001
            NMAX = 500
            GO TO 50
C
C      Example 2 (Non-Newtonian power law)
        12  EN = 0.7
            K = 100.*0.0000001465
            DP = 0.00001
            NMAX = 5000
            GO TO 50
C
C      Example 3 (Non-Newtonian power law)
C      Small DP and large NMAX finds PA with
less guess work
        14  EN = 0.7
            K = 100.*0.0000001465
            DP = 0.000001
            NMAX = 50000
            GO TO 50
C
C      Example 4 (Non-Newtonian power law)
        16  EN = 0.70
            K = 1700.*0.0000001450
            DP = 0.00001
            NMAX = 50000
            GO TO 50
C
C      Example 5 (Non-Newtonian power law)
        18  EN = 0.50
            K = 1700.*0.0000001450
            DP = 0.00001
            NMAX = 50000
            GO TO 50
C
C      More inputs ...

        50  QCCPS = 100.
            L2 = 20./2.54
            L3 = 20./2.54
            R2 = 1./2.54
            R3 = 1./2.54
            P2 = 2.
            P3 = 2.
C
C      Preliminaries ...
            EXPON = 1./EN
            PSTART = P3
            IF(P2.GE.PSTART) PSTART = P2
            PA = PSTART + DP
            WRITE(*,55)
        55  FORMAT(1X,'              N              PA
QTEST        QCCPS
           1     RATIO')
C      Testing PA values initializing ...
            DO 100 N = 1,NMAX
            TERM2 = EN*PI*R2**3.*((R2*(PA-
P2)/(2.*K*L2))**EXPON)/
           1       (3.*EN+1.)
            TERM3 = EN*PI*R3**3.*((R3*(PA-
P3)/(2.*K*L3))**EXPON)/
           1       (3.*EN+1.)
            QTEST = TERM2 + TERM3
            QCCPSTEST = 16.38706*QTEST
            RATIO = QCCPSTEST/QCCPS
            IF(RATIO.GT.0.99.AND.RATIO.LT.1.0)
           1WRITE(*,70) N,PA,QCCPSTEST,QCCPS,RATIO
        70  FORMAT(1X,I10,E14.6,2E12.4,F11.7)
            IF(RATIO.GT.1.0) THEN
            PA = PA - DP
```

```
      DP = DP/2.
      PA = PA + DP
      ERROR = 1. - RATIO
      IF(ERROR.LT.0.001) GO TO 105
      ENDIF
      PA = PA + DP
  100 CONTINUE
  105 STOP
      END
```

Figure 3-2. Power Law solution for junction pressure.

In the above source listing, the Power Law solution for junction pressure P_a (psi) is provided where Q_1 (cc/s) is given, with iterations developed in the "DO 100" loop. We now describe the iterative "half-step" solutions obtained for P_a. In Newtonian flow Example 1 immediately below, the assumed computational parameters are identical to those used in the exact solution underlying Figure 2-3. The final solution, highlighted in **bold** font, yields = 2.00373 psi, which also appears in Figure 2-3 for our assumed Q_1 = 100 cc/s (the "test Q" almost matches the given 100 cc/s). In the examples below, "N" is a numerical counter which records the "guess number" for P_a, whose value appears immediately to its right. As N increases, the ratio increases monotonically, with the calculations terminating once the RATIO reaches unity within a user-prescribed error bound. The computing histories are robust and stable. Despite the large Ns used for Examples 4 and 5, the desk time involved for a Windows i5 computer is less than one second.

```
C:\bifurc-4 <Return>

 Example 1-5?  Enter:  1

       N        PA          QTEST       QCCPS       RATIO
     369  0.200370E+01  0.9905E+02  0.1000E+03  0.9904621
     370  0.200371E+01  0.9931E+02  0.1000E+03  0.9931462
     371  0.200372E+01  0.9958E+02  0.1000E+03  0.9958304
     372  0.200373E+01  0.9985E+02  0.1000E+03  0.9985145
 Stop - Program terminated.

 Example 1-5?  Enter:  2

       N        PA          QTEST       QCCPS       RATIO
     .
    1146  0.201148E+01  0.9942E+02  0.1000E+03  0.9941543
    1147  0.201149E+01  0.9954E+02  0.1000E+03  0.9953938
    1148  0.201150E+01  0.9966E+02  0.1000E+03  0.9966338
    1149  0.201151E+01  0.9979E+02  0.1000E+03  0.9978743
    1150  0.201152E+01  0.9991E+02  0.1000E+03  0.9991152
 Stop - Program terminated.

 Example 1-5?  Enter:  3
       N        PA          QTEST       QCCPS       RATIO
   .
   12008  0.201145E+01  0.9912E+02  0.1000E+03  0.9912050
   12009  0.201145E+01  0.9913E+02  0.1000E+03  0.9913229
   12010  0.201145E+01  0.9914E+02  0.1000E+03  0.9914407
   .
   .
   12060  0.201150E+01  0.9973E+02  0.1000E+03  0.9973426
   12070  0.201151E+01  0.9985E+02  0.1000E+03  0.9985242
   12080  0.201152E+01  0.9997E+02  0.1000E+03  0.9997062
   12081  0.201152E+01  0.9998E+02  0.1000E+03  0.9998245
   12082  0.201152E+01  0.9999E+02  0.1000E+03  0.9999428
 Stop - Program terminated.
```

```
 Example 1-5?  Enter:  4

       N        PA          QTEST       QCCPS       RATIO
   19227  0.219253E+01  0.9901E+02  0.1000E+03  0.9900671
   19228  0.219254E+01  0.9901E+02  0.1000E+03  0.9901407
   19229  0.219255E+01  0.9902E+02  0.1000E+03  0.9902143
   19230  0.219256E+01  0.9903E+02  0.1000E+03  0.9902877
   .
   19330  0.219356E+01  0.9977E+02  0.1000E+03  0.9976528
   19340  0.219366E+01  0.9984E+02  0.1000E+03  0.9983900
   19350  0.219376E+01  0.9991E+02  0.1000E+03  0.9991276
   19360  0.219386E+01  0.9999E+02  0.1000E+03  0.9998654
   19361  0.219387E+01  0.9999E+02  0.1000E+03  0.9999391
 Stop - Program terminated.

 Example 1-5?  Enter:  5

       N        PA          QTEST       QCCPS       RATIO
   .
    8780  0.208792E+01  0.9991E+02  0.1000E+03  0.9991337
    8781  0.208793E+01  0.9994E+02  0.1000E+03  0.9993613
    8782  0.208794E+01  0.9996E+02  0.1000E+03  0.9995889
    8783  0.208795E+01  0.9998E+02  0.1000E+03  0.9998167
 Stop - Program terminated.
```

Having successfully found the junction pressure P_a , we evaluate Equations 3.3 – 3.9 for inlet pressure, branch flow rates and wall viscous shear stresses. In our **BIFURC-5** code (not shown), we added the logic below.

```
 105  PPSI1 = PA + (2.*K*L1/R1)*
     1       ((3.*EN+1.)*QIN3PS/(EN*PI*R1**3.))**EN
      Q1 = QCCPS
      Q2 = 16.38706*(EN*PI*R2**3./(3.*EN+1.))*
     1     (R2*(PA-P2)/(2.*K*L2))**EXPON
      Q3 = 16.38706*(EN*PI*R3**3./(3.*EN+1.))*
     1     (R3*(PA-P3)/(2.*K*L3))**EXPON
      TAU1 = (PPSI1 - PA)*R1/(2.*L1)
      TAU2 = (PA - P2)*R2/(2.*L2)
      TAU3 = (PA - P3)*R3/(2.*L3)
```

We re-run the Examples 1-5. In Example 1 below, we had considered a purely Newtonian flow with a 10 cp viscosity. Results were given in Figure 2-3 and are duplicated here.

```
C:\>BIFURC-5 <Return>

 Example 1-5?  Enter:  1

       N        PA          QTEST       QCCPS       RATIO
     370  0.200371E+01  0.9931E+02  0.1000E+03  0.9931462
     371  0.200372E+01  0.9958E+02  0.1000E+03  0.9958304
     372  0.200373E+01  0.9985E+02  0.1000E+03  0.9985145
     P1 = 2.0111911 (PSI)
     Q1 = 100.00, Q2 =  49.99, Q3 =  49.99 (CC/S)
     TAU1 = 0.00018653,TAU2 = 0.00009325, TAU3 =
0.00009325 (PSI)
 Stop - Program terminated.
```

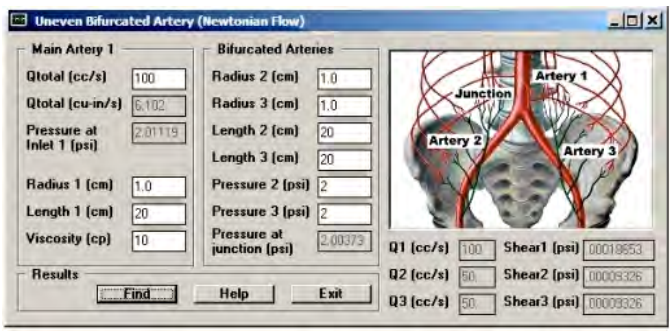

Figure 2-3. Calculated results appear in gray boxes.

Very good results are obtained. Earlier results were based on exact, closed form, analytical solutions using the Newtonian model, while here they follow from a "half-step" iterative scheme for Power Law fluids. The exact inlet pressure earlier was 2.01119 psi and the iterated value here is also 2.01119 psi. Also, the main flow is correctly divided into two branches having equal 49.99 cc/s (as compared to 50 cc/s) rates. Finally, the equal shear stresses in branches "2" and "3" agree with exact solutions to the fourth decimal place. Computed results for Examples 2-5 are given below.

```
     Example 1-5?  Enter:  2

            N        PA          QTEST       QCCPS      RATIO
          .
          .
          1148  0.201150E+01  0.9966E+02  0.1000E+03  0.9966338
          1149  0.201151E+01  0.9979E+02  0.1000E+03  0.9978743
          1150  0.201152E+01  0.9991E+02  0.1000E+03  0.9991152

           P1 = 2.0302393 (PSI)
           Q1 = 100.00, Q2 =  49.99, Q3 =  49.99 (CC/S)
           TAU1  =  0.00046797,  TAU2  =  0.00028802,  TAU3  =
0.00028802(PSI)
     Stop - Program terminated.

     Example 1-5?  Enter:  3

            N        PA          QTEST       QCCPS      RATIO
          .
          .
          12079  0.201152E+01  0.9996E+02  0.1000E+03  0.9995880
          12080  0.201152E+01  0.9997E+02  0.1000E+03  0.9997062
          12081  0.201152E+01  0.9998E+02  0.1000E+03  0.9998245
          12082  0.201152E+01  0.9999E+02  0.1000E+03  0.9999428

           P1 = 2.0302415 (PSI)
           Q1 = 100.00, Q2 =  50.00, Q3 =  50.00 (CC/S)
           TAU1  =  0.00046797,  TAU2  =  0.00028807,  TAU3  =
0.00028807(PSI)

     Stop - Program terminated.

     Example 1-5?  Enter:  4
            N        PA          QTEST       QCCPS      RATIO
          .
          19358  0.219384E+01  0.9997E+02  0.1000E+03  0.9997178
          19359  0.219385E+01  0.9998E+02  0.1000E+03  0.9997916
          19360  0.219386E+01  0.9999E+02  0.1000E+03  0.9998654
          19361  0.219387E+01  0.9999E+02  0.1000E+03  0.9999391

           P1 = 2.5088389 (PSI)
           Q1 = 100.00, Q2 =  50.00, Q3 =  50.00 (CC/S)
           TAU1  =  0.00787402,  TAU2  =  0.00484695,  TAU3  =
0.00484695(PSI)

     Stop - Program terminated.
     Example 1-5?  Enter:  5

            N        PA          QTEST       QCCPS      RATIO
          .
          .
          8779  0.208791E+01  0.9989E+02  0.1000E+03  0.9989061
          8780  0.208792E+01  0.9991E+02  0.1000E+03  0.9991337
          8781  0.208793E+01  0.9994E+02  0.1000E+03  0.9993613
          8782  0.208794E+01  0.9996E+02  0.1000E+03  0.9995889
          8783  0.208795E+01  0.9998E+02  0.1000E+03  0.9998167

           P1 = 2.2123446 (PSI)
           Q1 = 100.00, Q2 =  50.00, Q3 =  50.00 (CC/S)
           TAU1  =  0.00310976,  TAU2  =  0.00219886,  TAU3  =
0.00219886(PSI)

     Stop - Program terminated.
```

Although there are no Power Law solutions with which to benchmark the above results, the calculated inlet pressures and shear stresses appear to be correct in order-of-magnitude as compared with Newtonian results. The iterations are rapidly convergent and require less than a second on Windows i5 computers.

3.2 Herschel-Bulkley Fluids

In developing math formulations and numerical solutions, we importantly "start simple" and consider complications incrementally. Validation is key at each step. We had started with simple Newtonian flow, first considering a two-branch bifurcation with Q_1 specified initially, and then strategies for additional branches and Power Law fluids were considered.

3.2.1 Analytical and numerical approach

We first dealt with nonlinear Power Law fluids. Because exact, closed form, analytical solutions similar to those in Newtonian flow are not possible and Newton-Raphson root finder methods are not ideal, we devised a "half-step"approach, taking advantage of the monotonic relation between pressure gradient and flow rate. This method was validated against exact analytical results using a Newtonian example; such fluids represent one limit of the more general Power Law flow. We now consider Herschel-Bulkley fluids, which extend Power Law models to include yield stress. The mathematics are more involved, so we similarly validate new results against earlier Newtonian *and* Power Law calculations.

Yield stress modeling. The classical Herschel-Bulkley pipe flow model combines Power Law with yield stress (τ_y) characteristics, with the result that

$$\tau = \tau_y + k\,(-dU/dr)^n \tag{3.10}$$

$$U(r) = k^{-1/n}\,(\Delta P/2L)^{-1}\,\{n/(n+1)\} \times [(R\Delta P/2L - \tau_y)^{(n+1)/n} - (r\Delta P/2L - \tau_y)^{(n+1)/n}],\ R_p \le r \le R \tag{3.11}$$

$$U(r) = k^{-1/n}\,(\Delta P/2L)^{-1}\,\{n/(n+1)\} \times [(R\Delta P/2L - \tau_y)^{(n+1)/n} - (R_p\,\Delta P/2L - \tau_y)^{(n+1)/n}],\ 0 \le r \le R_p \tag{3.12}$$

$$R_p = 2\tau_y\,L/\Delta P \tag{3.13}$$

$$Q/(\pi R^3) = k^{-1/n}\,(R\Delta P/2L)^{-3}\,(R\Delta P/2L - \tau_y)^{(n+1)/n} \times [(R\Delta P/2L - \tau_y)^2\,n/(3n+1) + 2\,\tau_y\,(R\Delta P/2L - \tau_y)\,n/(2n+1) + \tau_y^2\,n/(n+1)] \tag{3.14}$$

Here, the conventional "plug radius" R_p defines the outer extent of a solid moving cylinder, which resides at the center of the pipe. Because the flows that are less than and greater than this radius are different, two solutions for the axial velocity U(r) appear above. Our usual starting point, namely, mass conservation assuming "$Q_1 = Q_2 + Q_3$," requires first a volume integration of the axial velocity U(r) to produce volume flow rate Q(r), and second, the explicit representation

$$Q_1 =$$
$$\pi R_2^3\, k^{-1/n} \left(R_2(P_a - P_2)/2L_2\right)^{-3} \left(R_2(P_a - P_2)/2L_2 - \tau_y\right)^{(n+1)/n}$$
$$\times \left[(R_2(P_a - P_2)/2L_2 - \tau_y)^2\, n/(3n+1)\right.$$
$$+ \left. 2\,\tau_y\,(R_2(P_a - P_2)/2L_2 - \tau_y)\, n/(2n+1) + \tau_y^2\, n/(n+1)\right]$$
$$+ \pi R_3^3\, k^{-1/n} \left(R_3(P_a - P_3)/2L_3\right)^{-3} \left(R_3(P_a - P_3)/2L_3 - \tau_y\right)^{(n+1)/n}$$
$$\times \left[(R_3(P_a - P_3)/2L_3 - \tau_y)^2\, n/(3n+1)\right.$$
$$+ \left. 2\,\tau_y\,(R_3(P_a - P_3)/2L_3 - \tau_y)\, n/(2n+1) + \tau_y^2\, n/(n+1)\right] \quad (3.15)$$

For Power Law flows, the relation corresponding to Equation 3.15, namely Equation 3.2, was solved by a "half-step" method to produce a solution for junction pressure P_a. Then, Equation 3.1 for the general expression $Q = \{n\pi R^3/(3n + 1)\}\,[R(P_i - P_o)/(2kL)]^{1/n}$ was written for branch "1" in the form "$Q_1 = \{nR_1^3/(3n + 1)\}\,[R_1\,(P_i - P_a)/(2kL_1)]^{1/n}$ " and analytically solved to give the inlet pressure in Equation 3.6.

For Herschel-Bulkley fluids, the basic expression for flow rate is more complicated. Equation 3.15 is still solved as before in the Power Law case for the *junction* pressure P_a, but an analytical *inlet* pressure solution such as that in Equation 3.6 is not possible because of nonlinearities. However, a numerical solution can be obtained if we write Equation 3.14 for branch "1," that is,

$$Q_1/(\pi R^3) =$$
$$k^{-1/n} \left(R_1(P_i - P_a)/2L_1\right)^{-3} \left(R_1(P_i - P_a)/2L_1 - \tau_y\right)^{(n+1)/n} \quad (3.16)$$
$$\times \left[(R_1(P_i - P_a)/2L_1 - \tau_y)^2\, n/(3n+1)\right.$$
$$+ \left. 2\,\tau_y\,(R_1(P_i - P_a)/2L_1 - \tau_y)\, n/(2n+1) + \tau_y^2\, n/(n+1)\right]$$

and solve for P_i by also using a half-step approach. In summary, Q_1 is prescribed, while Q_2 and Q_3 are given by the first-three and second-three lines, respectively, of Equation 3.15. As before, the shear stresses are

$$\tau_1 = (P_i - P_a)\;\; R_1/(2L_1) \quad (3.17)$$

$$\tau_2 = (P_a - P_{o,2})\; R_2/(2L_2) \quad (3.18)$$

$$\tau_3 = (P_a - P_{o,3})\; R_3/(2L_3) \quad (3.19)$$

These follow from the global force balance given by "$\pi R^2 \Delta P = \tau_w\,(2\pi RL)$," noting that τ_y yield stress effects have already been considered in the calculations for pressure in Equations 3.15 and 3.16. As before, we proceed with validations and re-run Examples 1-5 from our Power Law results, first for the zero yield stress case. Because the Power Law and Herschel-Bulkley equations and algorithms are completely different and solved by independently written programs, agreement with prior results, and with earlier Newtonian results, guarantees correctness. BIFURC-6 Fortran source code (not shown) provides the full suite of solutions for P_a, P_i, volume flow rate and viscous shear stress with yield effects (this solver also applies to Bingham Plastics for all k and τ_y values if we set n = 1).

3.2.2 BIFURC-6 runs for τ_y = 0 psi (Power Law limit)

```
C:\>bifurc-6 <Return>
Example 1-5?  Enter:  1

 Solving for junction pressure PA ...

  N        PA          QTEST       QCCPS       RATIO
 369  0.200370E+01  0.9905E+02  0.1000E+03  0.9904621
 370  0.200371E+01  0.9931E+02  0.1000E+03  0.9931461
 371  0.200372E+01  0.9958E+02  0.1000E+03  0.9958305
 372  0.200373E+01  0.9985E+02  0.1000E+03  0.9985147

 Solving for Q1 inlet pressure P1 ...

  N      PINLET        QTEST       QCCPS       RATIO
1477  0.201112E+01  0.9906E+02  0.1000E+03  0.9905897
1478  0.201113E+01  0.9913E+02  0.1000E+03  0.9912611
1479  0.201113E+01  0.9919E+02  0.1000E+03  0.9919319
.
.
1480  0.201114E+01  0.9926E+02  0.1000E+03  0.9926032
1490  0.201119E+01  0.9993E+02  0.1000E+03  0.9993138
1491  0.201119E+01  0.1000E+03  0.1000E+03  0.9999846

 Additional calculated quantities ...

 P1 = 2.0111935 (PSI)
 Q1 = 100.00, Q2 =  50.06, Q3 =  50.06 (CC/S)
 TAU1  =  0.00018659,  TAU2  =  0.00009325,  TAU3  =
0.00009325(PSI)

Stop - Program terminated.
```

The above results agree to the fourth decimal place with those in Figure 2-3 obtained using the exact Newtonian model and to those in Section 3.1 using the Power Law model. The results of Examples 2–5 here also agree with those in Section 3.1 to about four places. This validates the "zero yield stress" limit of our solutions.

```
Example 1-5?  Enter:  2

 Solving for junction pressure PA ...

  N        PA          QTEST       QCCPS       RATIO
.
1148  0.201150E+01  0.9966E+02  0.1000E+03  0.9966335
1149  0.201151E+01  0.9979E+02  0.1000E+03  0.9978742
1150  0.201152E+01  0.9991E+02  0.1000E+03  0.9991152

 Solving for Q1 inlet pressure P1 ...

  N      PINLET        QTEST       QCCPS       RATIO
3714  0.203011E+01  0.9903E+02  0.1000E+03  0.9902756
3715  0.203012E+01  0.9907E+02  0.1000E+03  0.9906565
.
.
3736  0.203022E+01  0.9987E+02  0.1000E+03  0.9986679
3737  0.203023E+01  0.9990E+02  0.1000E+03  0.9990498
3738  0.203023E+01  0.9994E+02  0.1000E+03  0.9994319
3739  0.203024E+01  0.9998E+02  0.1000E+03  0.9998142

  Additional calculated quantities ...

 P1 = 2.0302393 (PSI)
Q1 = 100.00, Q2 =  50.02, Q3 =  50.02 (CC/S)
TAU1  =  0.00046797,  TAU2  =  0.00028802,  TAU3  =
0.00028802(PSI)

Stop - Program terminated.
```

```
    Example 1-5?  Enter:  3

     Solving for junction pressure PA ...

      N        PA          QTEST       QCCPS       RATIO
    .
   12080  0.201152E+01  0.9997E+02  0.1000E+03  0.9997062
   12081  0.201152E+01  0.9998E+02  0.1000E+03  0.9998245
   12082  0.201152E+01  0.9999E+02  0.1000E+03  0.9999426

     Solving for Q1 inlet pressure P1 ...

      N      PINLET        QTEST       QCCPS       RATIO
    .
   39252  0.203024E+01  0.9999E+02  0.1000E+03  0.9998869
   39253  0.203024E+01  0.9999E+02  0.1000E+03  0.9999232
   39254  0.203024E+01  0.1000E+03  0.1000E+03  0.9999595
   39255  0.203024E+01  0.1000E+03  0.1000E+03  0.9999962

      Additional calculated quantities ...

     P1 = 2.0302417 (PSI)
     Q1 = 100.00, Q2 =  50.00, Q3 =  50.00 (CC/S)
     TAU1   =   0.00046797,   TAU2   =   0.00028807,   TAU3   =
0.00028807(PSI)

    Stop - Program terminated.

    Example 1-5?  Enter:  4

     Solving for junction pressure PA ...

      N        PA          QTEST       QCCPS       RATIO
    .
   19350  0.219376E+01  0.9991E+02  0.1000E+03  0.9991276
   19360  0.219386E+01  0.9999E+02  0.1000E+03  0.9998652
   19361  0.219387E+01  0.9999E+02  0.1000E+03  0.9999392

     Solving for Q1 inlet pressure P1 ...

      N      PINLET        QTEST       QCCPS       RATIO
    .
   62900  0.250880E+01  0.9998E+02  0.1000E+03  0.9998283
   62905  0.250883E+01  0.9999E+02  0.1000E+03  0.9999418
   62906  0.250883E+01  0.1000E+03  0.1000E+03  0.9999645
   62907  0.250884E+01  0.1000E+03  0.1000E+03  0.9999871

      Additional calculated quantities ...

     P1 = 2.5088384 (PSI)
     Q1 = 100.00, Q2 =  50.00, Q3 =  50.00 (CC/S)
     TAU1   =   0.00787401,   TAU2   =   0.00484695,   TAU3   =
0.00484695(PSI)

    Stop - Program terminated.

    Example 1-5?  Enter:  5

     Solving for junction pressure PA ...

      N        PA          QTEST       QCCPS       RATIO
    .
    8781  0.208793E+01  0.9994E+02  0.1000E+03  0.9993613
    8782  0.208794E+01  0.9996E+02  0.1000E+03  0.9995888
    8783  0.208795E+01  0.9998E+02  0.1000E+03  0.9998168

     Solving for Q1 inlet pressure P1 ...

      N      PINLET        QTEST       QCCPS       RATIO
    .
   24842  0.221233E+01  0.9997E+02  0.1000E+03  0.9997455
   24843  0.221233E+01  0.9998E+02  0.1000E+03  0.9998258
   24844  0.221234E+01  0.9999E+02  0.1000E+03  0.9999064
   24845  0.221234E+01  0.1000E+03  0.1000E+03  0.9999870

      Additional calculated quantities ...

     P1 = 2.2123463 (PSI)
     Q1 = 100.00, Q2 =  50.00, Q3 =  50.00 (CC/S)
     TAU1   =   0.00310980,   TAU2   =   0.00219886,   TAU3   =
0.00219886(PSI)

    Stop - Program terminated.
```

3.2.3 BIFURC-6 runs assuming τ_y = 0.00001 psi

Having validated our zero yield stress results, we turn to simulations with non-zero yield stress. We will re-run Examples 1-5 with a yield of 0.00001 psi, which is consistent with certain medical diagnostic examples, for example, Lee, Xue, Nam, Lim and Shin (2011). This larger value is not too much more than the values observed clinically but was chosen for numerical study purposes.

```
C:\>bifurc-6-yield-stress <Return>

    Example 1-5?  Enter:  1

     Solving for junction pressure PA ...

      N        PA          QTEST       QCCPS       RATIO
    .
    383  0.200424E+01  0.9923E+02  0.1000E+03  0.9923480
    384  0.200425E+01  0.9950E+02  0.1000E+03  0.9950320
    385  0.200426E+01  0.9977E+02  0.1000E+03  0.9977157

     Solving for Q1 inlet pressure P1 ...

      N      PINLET        QTEST       QCCPS       RATIO
    .
   1514  0.201224E+01  0.9976E+02  0.1000E+03  0.9975594
   1515  0.201224E+01  0.9982E+02  0.1000E+03  0.9982303
   1516  0.201225E+01  0.9989E+02  0.1000E+03  0.9989014
   1517  0.201225E+01  0.9996E+02  0.1000E+03  0.9995728

      Additional calculated quantities ...

     P1 = 2.0122540 (PSI)
     Q1 = 100.00, Q2 =  50.02, Q3 =  50.02 (CC/S)
     TAU1   =   0.00019984,   TAU2   =   0.00010651,   TAU3   =
0.00010651(PSI)

    Stop - Program terminated.

    Example 1-5?  Enter:  2

     Solving for junction pressure PA ...

      N        PA          QTEST       QCCPS       RATIO
    .
   1160  0.201202E+01  0.9971E+02  0.1000E+03  0.9971333
   1161  0.201203E+01  0.9984E+02  0.1000E+03  0.9983738
   1162  0.201204E+01  0.9996E+02  0.1000E+03  0.9996150

     Solving for Q1 inlet pressure P1 ...

      N      PINLET        QTEST       QCCPS       RATIO
    .
   3759  0.203126E+01  0.9986E+02  0.1000E+03  0.9985799
   3760  0.203126E+01  0.9990E+02  0.1000E+03  0.9989616
   3761  0.203127E+01  0.9993E+02  0.1000E+03  0.9993436
   3762  0.203127E+01  0.9997E+02  0.1000E+03  0.9997258

      Additional calculated quantities ...

     P1 = 2.0312748 (PSI)
     Q1 = 100.00, Q2 =  50.04, Q3 =  50.04 (CC/S)
     TAU1   =   0.00048085,   TAU2   =   0.00030102,   TAU3   =
0.00030102(PSI)

    Stop - Program terminated.
```

```
 Example 1-5?  Enter:  3

  Solving for junction pressure PA ...

    N        PA          QTEST       QCCPS       RATIO
.
12202  0.201204E+01  0.9997E+02  0.1000E+03  0.9997334
12203  0.201204E+01  0.9999E+02  0.1000E+03  0.9998513
12204  0.201204E+01  0.1000E+03  0.1000E+03  0.9999695

  Solving for Q1 inlet pressure P1 ...

    N      PINLET        QTEST       QCCPS       RATIO
.
39496  0.203127E+01  0.9999E+02  0.1000E+03  0.9998897
39497  0.203127E+01  0.9999E+02  0.1000E+03  0.9999259
39498  0.203127E+01  0.1000E+03  0.1000E+03  0.9999623
39499  0.203127E+01  0.1000E+03  0.1000E+03  0.9999988

   Additional calculated quantities ...

  P1 = 2.0312746 (PSI)
  Q1 = 100.00, Q2 =  50.00, Q3 =  50.00 (CC/S)
  TAU1  =  0.00048088,  TAU2  =  0.00030098,  TAU3  =
0.00030098(PSI)

 Stop - Program terminated.
```

It is interesting to compare Example 1 (where the yield stress is zero) with Example 1 here (where the yield is 0.00001 psi). In the former case, P_a and P_i are 2.00373 and 2.01119 psi, while here, they are 2.00426 and 2.01225 psi. It is more meaningful to subtract the background "2 psi," to compare 0.00373 with 0.00426, and 0.01119 with 0.01225. The percent increases are 14% and 9% respectively, which are large considering that $\tau_y = 0.00001$ psi.

```
 Example 1-5?  Enter:  4

   Solving for junction pressure PA ...

    N        PA          QTEST       QCCPS       RATIO
.
19371  0.219437E+01  0.9998E+02  0.1000E+03  0.9998180
19372  0.219438E+01  0.9999E+02  0.1000E+03  0.9998918
19373  0.219439E+01  0.1000E+03  0.1000E+03  0.9999657

   Solving for Q1 inlet pressure P1 ...

    N      PINLET        QTEST       QCCPS       RATIO
.
62927  0.250986E+01  0.9999E+02  0.1000E+03  0.9999125
62928  0.250986E+01  0.9999E+02  0.1000E+03  0.9999353
62929  0.250987E+01  0.1000E+03  0.1000E+03  0.9999578
62930  0.250987E+01  0.1000E+03  0.1000E+03  0.9999806

   Additional calculated quantities ...

  P1 = 2.5098739 (PSI)
  Q1 = 100.00, Q2 =  50.00, Q3 =  50.00 (CC/S)
  TAU1  =  0.00788689,  TAU2  =  0.00485995,  TAU3  =
0.00485995(PSI)

 Stop - Program terminated.
```

```
 Example 1-5?  Enter:  5
   Solving for junction pressure PA ...

    N        PA          QTEST       QCCPS       RATIO
.
 8791  0.208843E+01  0.9994E+02  0.1000E+03  0.9993680
 8792  0.208844E+01  0.9996E+02  0.1000E+03  0.9995956
 8793  0.208845E+01  0.9998E+02  0.1000E+03  0.9998235

   Solving for Q1 inlet pressure P1 ...

    N      PINLET        QTEST       QCCPS       RATIO
.
24862  0.221333E+01  0.9997E+02  0.1000E+03  0.9997498
24863  0.221333E+01  0.9998E+02  0.1000E+03  0.9998301
24864  0.221334E+01  0.9999E+02  0.1000E+03  0.9999106
24865  0.221334E+01  0.1000E+03  0.1000E+03  0.9999914

    Additional calculated quantities ...

  P1 = 2.2133467 (PSI)
  Q1 = 100.00, Q2 =  50.00, Q3 =  50.00 (CC/S)
  TAU1  =  0.00312231,  TAU2  =  0.00221136,  TAU3  =
0.00221136(PSI)

 Stop - Program terminated.
```

In summary, note that the number of evaluations "N" have exceeded 60,000 in some runs. In others not reported here, they approach 200,000. This large number arises because we chose extremely small ΔP increments to obtain high accuracy solutions. Nonetheless, all cases required less than one second on Windows i5 machines. In this work, it was important to evaluate numerical stability in the half-step approach, plus robustness and the ability to capture four decimal place accuracy in pressures and viscous stresses.

3.3 Newtonian and Herschel-Bulkley Examples

We studied blood flows in arteries because they can be both Newtonian and non-Newtonian. For the former, the viscosity μ is always constant. The same value applies regardless of flow rate, radius, position within the artery, or even changes in cross-sectional shape. It is easily measured and its meaning is well understood. For instance, the Hagen-Poiseuille formula $Q = \pi R^4 (P_i - P_o) / (8\mu L)$ shows how doubling μ will reduce Q by half and how doubling pressure gradient will double Q. These benefits are lost in non-Newtonian flows.

In Example 1 for Newtonian flow, Table 1 shows exact solutions useful in studying flow blockage. We assume μ = 10 cp, Q_1 = 100 cc/s, R_1 = 1.52 cm, L_1 = 40 cm, $R_2 = R_3$ = 0.89 cm, $L_2 = L_3$ = 20 cm, and $P_2 = P_3$ = 2 psi. We have tabulated P_1, P_a, τ_1 and τ_2 (= τ_3) for simple clogs with decreasing flow areas (found by *reducing radii* successively by 10%) to model worsening conditions. The results in Runs 8-10 show how severe consequences are expected at the higher blockage levels. Of course, irregular blockages would be more realistic than concentric ones, but our purpose here is to emphasize the severities associated with large blockages.

Table 1. Example 1 – *Newtonian* results for aorta and iliac arteries.

Run	Area Open	P_1 (psi)	P_a (psi)	τ_1 (psi)	τ_2 , τ_3 (psi)
1	100%	2.0086	2.0057	0.000055	0.00013
2	81%	2.013	2.0086	0.000076	0.00018
3	64%	2.021	2.014	0.00011	0.00025
4	49%	2.036	2.024	0.00016	0.00037
5	36%	2.067	2.044	0.00026	0.00059
6	25%	2.14	2.091	0.00044	0.0010
7	16%	2.34	2.22	0.00086	0.0020
8	9%	3.07	2.70	0.0020	0.0047
9	4%	7.39	5.55	0.0069	0.016
10	1%	88.3	58.9	0.55	0.13

As blood vessel diameters decrease, non-Newtonian effects become important. The behavior of the "apparent viscosity η," that is, the proportionality between viscous shear stress and shear rate in "$\tau = \eta\, d\gamma/dt$," is less clear. Unlike its Newtonian counterpart, η depends on flow rate, pressure drop, conduit size and shape, and so on. This means that blood viscosity will vary with local radius, pressure gradient, flow rate, geometric deformations and position in the cross-section. Thus, the η obtained from a specific lab viscometer shear rate may not be directly relevant to a diagnosis, so the use of apparent viscosity for comparative assessments can be ambiguous. Such ideas are well known in drilling practice.

However, the use of "n and k" and "n, k and τ_y" for Power Law and Herschel-Bulkley fluids is unambiguous, because these constants represent true properties of the fluid. Together with Q_1, P_2, P_3 and the input geometry, parameters which will vary from case to case, the quantities P_1, P_a, τ_1, τ_2 and τ_3 particular to each scenario can be derived. In all areas of science, whether they are biological or related to drilling and cementing, it is more meaningful to study physical attributes that have dynamical importance rather than ill-defined viscometer viscosities with limited application. Preferred properties include pressure levels that affect bursting, pressure gradients related to flow efficiency, wall shear stresses that influence long-term wear and tear, and possible ratios like Q_2/Q_3 that may affect overall bodily functions.

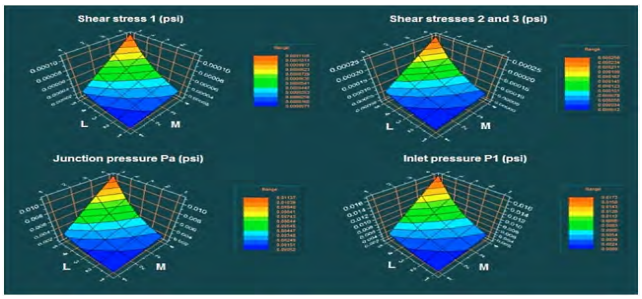

Figure 3-3. Example 2 – *Power Law* results for P_1, P_a, τ_1 and τ_2 ($= \tau_3$).

In Example 2 for Power Law fluids, we focus less on viscosity and more on actual properties as they depend on n and k. We assume Q_1 = 100 cc/s, R_1 = 1.52 cm, L_1 = 40 cm, $R_2 = R_3$ = 0.89 cm, $L_2 = L_3$ = 20 cm, $P_2 = P_3$ = 2 psi and τ_y = 0 psi. Typical results, based on published n and k health data, appear in Figure 3-3 (in the pressure plots, the background 2 psi is removed to highlight dynamic effects). The plotting index L = 1 to 5 corresponds to n = 0.6 to 1.0, while that for M = 1 to 4 corresponds to k = 0.0000007325 to 0.000002930 (note that L = 5, M = 1 corresponds to a reference 5 cp Newtonian fluid). Herschel-Bulkley solutions for τ_y = 0.000001 psi showed very slight pressure and stress increases, so the corresponding figures are not plotted.

Non-Newtonian effects, including yield stresses, are more pronounced in narrower diameters. In Example 3 for Herschel-Bulkley fluids, instead of repeating Example 2 with a nonzero τ_y value, we consider a system with smaller radii, both with and without yield stress. Comparative results for τ_y = 0 and a large value of τ_y = 0.00001 psi given in Figure 3-4 show relative magnitudes. Calculated wall shear stresses in all cases are within the ranges cited in published clinical data.

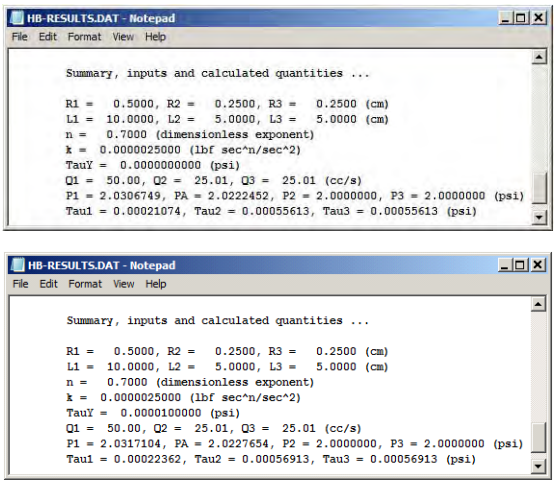

Figure 3-4. Example 3 – *Herschel-Bulkley* yield stress effects (tabulated results given as changes are visually imperceptible).

Power Law model limitations are well known in the literature. For example, the dimensions of "k" depend on the "n" value – thus, for graphs like those in Figure 3-3, k values must not be compared when n values differ. In our work, the plots suggested another deficiency in the Power Law model. The formula $Q = \{n\pi R^3/(3n + 1)\}\ [R(P_i - P_o)/(2kL)]^{1/n}$, reducing to Hagen-Poiseuille's law with $k = \mu$ when $n = 1$, is accepted in Newtonian flow. But suppose that Q is fixed, as is the case in blood flow studies. As $n \rightarrow 0$, use of L'Hospital's Rule leads to a questionable pressure gradient $(P_i - P_o)/L = 2k/R$ which is unrealistically independent of Q_1. This can be validated by direct calculations. Thus, caution is suggested in rate-constrained problems with small values of n – fortunately, n will typically exceed 0.7 in many applications.

4. Arbitrary Clogs in Bifurcated Pipelines

4.1 Motivating questions and examples

Earlier work (Chin, 2022) considered clogs of general cross-section in single-element pipes. In the above section, we studied pipe flows with general geometric bifurcations. These latter birurcation models, which apply to Newtonian, Power Law, Bingham Plastic and Herschel-Bulkley fluids, are extendable to other rheologies whenever flow rate versus pressure drop expressions are available. However, these relations are often restricted to circular geometries, thus imposing potential limitations for our method in applications.

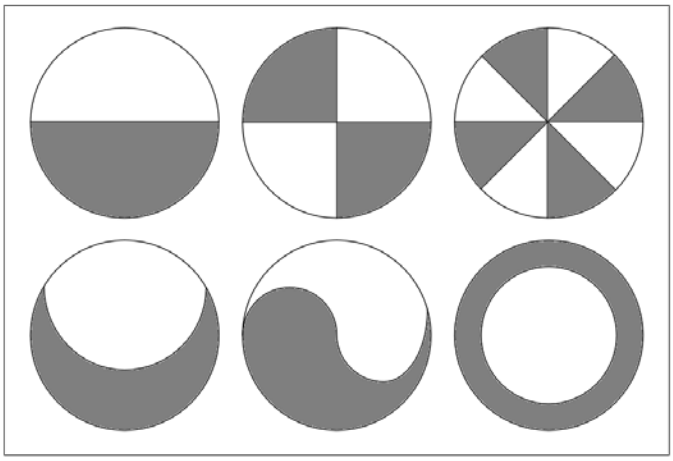

Figure 4-1. Possible 50% blocked configurations.

Here, we ask, "Is there a formalism by which circular cross-section bifurcation models can be used in problems where specific pipe elements are blocked by asymmetric clogs?" A simple (but incorrect) method is often suggested to solve even the simplest single-element problem. The approach consists in using standard formulas, for example, in Newtonian flow the Hagen-Poiseuille law, but replacing the actual radius by a simple geometrically defined "equivalent radius." This method, however, is subject to pitfalls.

For argument's sake, consider any of the real-world clogs in Figure 1-1 and suppose that it is associated with a 50% area blockage for a circular area A. The proposed method might require using an effective radius defined by $\pi R_{eff}^{\ 2} = A/2$ so that $R_{eff} = (A/2\pi)^{1/2}$. This radius would be used in the Hagen-Poiseuille law (or equivalent circle relation for other rheologies) to calculate shear stresses, pressure drops and so on. However, the method is incorrect because clog surface area and local inclinations exposed to frictional rubbing, important to determining flow properties unique to that clog, are completely ignored. For example, Figure 4-1 shows different 50% blocked configurations, each of which would obviously possess flow properties *different* from the others, and each of which could be solved unambiguously and exactly by mapping methods (Chin 2022). It is clear that actual flow rates (for a fixed pressure gradient) for the six Figure 4-1 flows are unlikely to satisfy an arbitrarily defined $R_{eff} = (A/2\pi)^{1/2}$ based only on geometric arguments – nor are any of the flows likely to share the same flow rate. In other words, over-simplified effective radii methods are not justified physically and should not be used. In the next section, we illustrate the above ideas with practical calculated results.

4.2 Detailed single-element pipe flow solutions

In the three examples below, we assume a Newtonian liquid with a viscosity of 1 cp, a volume flow rate of 100 gpm, and an outer radius of 3 inches. We will calculate the required axial pressure gradient using a half-step iteration together with our numerical mapping method (Chin 2022). Typical computing times are less than 1 sec per example on Windows i5 computers. Figure 4-2a shows the computed velocity distribution for a completely unclogged pipe, where red represents the rapid center flow and blue denotes the low speed flow next to the solid pipe wall. Because the outer boundary is a perfect circle, the exact Hagen-Poiseuille solution also applies, as shown in Figure 4-2b. Both runs yield the same pressure gradient of 0.00002136 psi/ft.

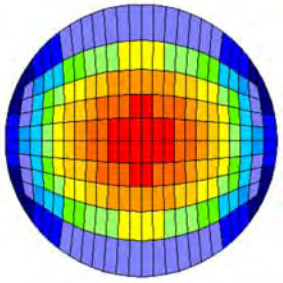

```
Axial pressure gradient of .2136E-04 psi/ft
yields volume flow rate of .1002E+03 gal/min.
Cross - sectional  area:  .2823E+02 sqr inch
```

Figure 4-2a. Fully circular un-clogged pipe with quadrilateral curvilinear internal boundary conforming meshes – conventional circular polar coordinates are *not* used.

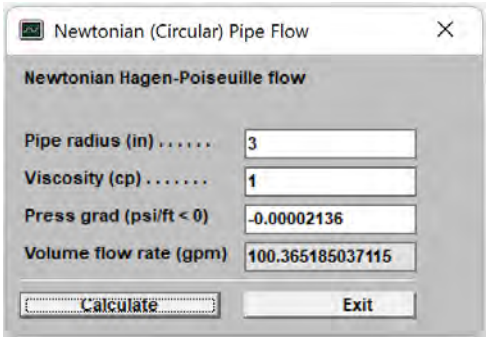

Figure 4-2b. Exact Hagen-Poiseuille solution for Fig. 4-2a.

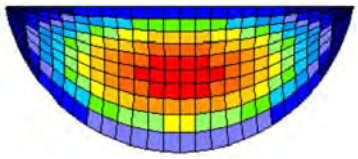

```
Axial pressure gradient of .2136E-03 psi/ft
yields volume flow rate of .9994E+02 gal/min.
Cross - sectional  area:  .1083E+02 sqr inch
```

Figure 4-2c. 60% clogged pipe, straight interface.

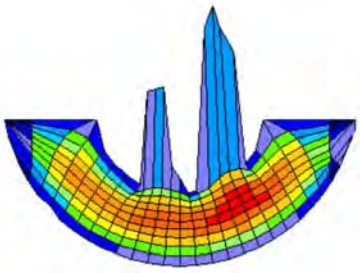

```
Axial pressure gradient of .5005E-03 psi/ft
yields volume flow rate of .1008E+03 gal/min.
Cross - sectional  area:  .1083E+02 sqr inch
```

Figure 4-2d. 60% clogged pipe, with erratic clog interface.

In Figure 4-2c, let us re-consider the circular pipe of Figure 4-2 by introducing a 60% straight blockage. Note that the pressure gradient, using our validated mapping method, increases from 0.00002136 psi/ft to 0.0002136 psi/ft (or ten-fold) in this case. This increase is much greater than that predicted on a geometric area-reduction basis alone. This shows that the "$\text{Speed}_1 \times \text{Area}_1 = \text{Speed}_2 \times \text{Area}_2$" formula in elementary fluid mechanics courses is not realistic since friction is ignored. Next, in Figure 4-2d, we consider a problem with an *identical* flow area as in Figure 4-2c. Here the pressure gradient increases from 0.0002136 psi/ft to 0.0005005 psi/ft (or more than double). The reason is physically apparent. The increased surface area at the clog interface increases the viscous friction acting on the common surface, so that larger pressure forces are required to drive the fluid at the same flow rate. This clearly demonstrates how "area alone" methods for effective radius definition suffer in accuracy. However, the concept behind an "effective radius" *can* play an important role in practical calculations if it is based on physics based arguments. The single-element method provides such a foundation (Chin 2022). For example, the mapping *does* allow prescription of no-slip velocity conditions on all solid wall and clog interfaces. And it *would* provide different solutions with different rate versus pressure relations for the top left and bottom three geometries of Figure 4-1. This provides the rationale for an effective radius based on a sound physical model. We suggest such a model by way of example.

4.3 Method for bifurcated systems with clogged piping elements

In this section, we create a simple example showing how both single-element clog and multi-element bifurcation models can be used in a practical application. Figure 4-3 uses the exact Hagen-Poiseuille solution for circular pipes to define effective radii for Figures 4-2c and 4-2d. In each case, the pressure gradient calculated using the exact mesh approach for the clog being considered is assumed and the effective radius for the fixed volume flow rate is calculated. The results show that R_{eff} = 1.686 inch (4.282 cm) for the clogged pipe in Figure 4-2c, while we have a smaller R_{eff} = 1.363 inch (3.462 cm) for the clog in Figure 4-2d.

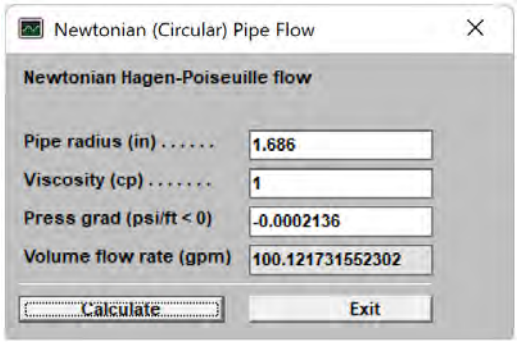

R_{eff} = 1.686 inch for clog in Figure 4-2c.

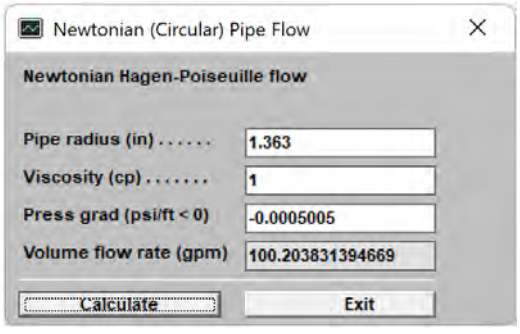

R_{eff} = 1.363 inch for clog in Figure 4-2d.

Figure 4-3. Effective radius calculations.

Now imagine a hypothetical problem with three elements where a single pipe branches into two pipes. All three are identical, with radii of 3 inch (7.62 cm) and lengths of 100 inch (254 cm). The inlet flow rate is 100 gpm (6,309 cc/s) as in the prior examples. The software for this three-element problem, discussed previously and shown again in Figure 4-4, was originally developed for biomedical applications. Aside from the labels and graphics shown, the flow equations and results are identical to those for engineering analysis. An outlet pressure of zero is used so that pressure drops can be directly read from the inlet pressure box. Note that white boxes accept data inputs while gray non-editable boxes represent calculated results. The upper screen shows a pressure of 0.00027 psi, while the results at the bottom right for flow rate and shear stress show expected agreement between both outlet pipes.

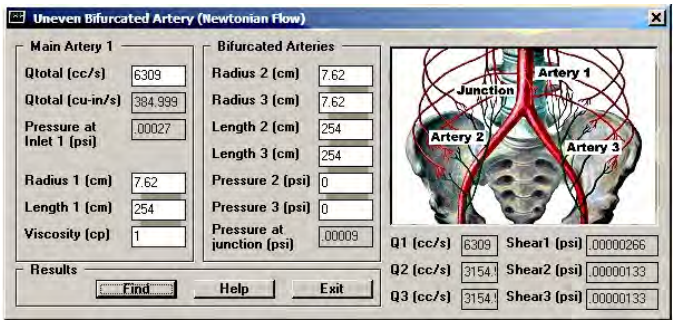

Model for perfect flow without clogs anywhere.

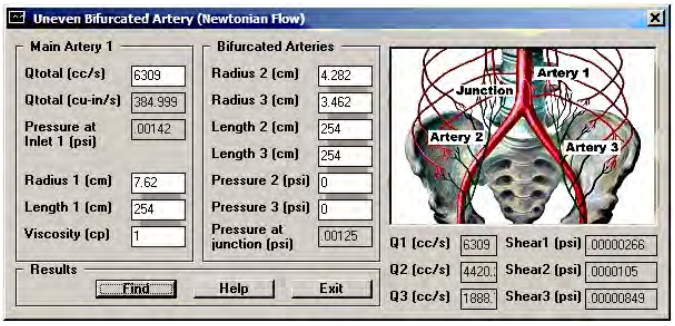

Model for unclogged inlet pipe with the clog of Figure 4-2c as element "2" and the clog of Figure 4-2d as element "3."

Figure 4-4. Calculated bifurcated pipe results.

We now suppose that pipe elements 2 and 3 are somehow clogged differently. In particular, the flow is unblocked in the feeder pipe, but clogged as in Figure 4-2c for element "2" and Figure 4-2d for element "3." Note how the original inlet pressure of 0.00027 psi has increased to 0.00142 psi (or more than five-fold). Moreover, from the bottom right in the lower screen of Figure 4-4, the volume flow rate in "2" is twice that of "3." Complementary shear stress results are also shown. We emphasize that the method shown above can also be applied to Power Law, Bingham Plastic and Herschel-Bulkley rheologies.

5. Discussion and Conclusions

This paper integrates two pipe models presented earlier (Chin 2022; Chin and Chin (2022). The first considers single-element pipes with arbitrary flow cross-sections and solves for detailed flow attributes on boundary-conforming, curvilinear meshes. The second solves for bifurcated pipe flow systems but assumes that all piping elements are circular in nature. We have provided highlights of both papers and in Section 4 demonstrated how the approaches can be integrated to solve bifurcated pipe applications where piping elements are arbitrarily clogged. The method is based on a physically sound "effective radius" approach in which the action of viscous shear stresses acting on all clog interfaces is accounted for. While we have shown how the procedure would be applied in a practical engineering application for Newtonian flow, where results could be validated step by step, the general approach also applies to Power Law, Bingham Plastic and Herschel-Bulkley rheologies. The method is credible and plausible from an engineering perspective. We might note that three-dimensional finite element analyses will provide greater flow detail, although involving greater cost, effort and computing resources. Finally, we note that the earlier papers explain how time-dependent clog modeling can be incorporated in our procedures. For details, the reader is referred to those references. The authors hope that these three papers will contribute to more accurate and convenient calculations in both engineering and biological sciences.

About the Authors.

Jamie is a Program Analyst with Stratamagnetic Software, LLC. In addition to pipe flow and petroleum engineering applications, she is interested in biological fluid mechanics and has applied pipe flow and bifurcation models to systems of arteries, capillaries and veins with tissue interaction.

Michael is Marketing Manager with Stratamagnetic Software, LLC in Houston, Texas. He brings significant insight to pipe flow analysis, with related experience in drilling fluids and Measurement While Drilling development at Halliburton, GE Oil & Gas and other industry leaders.

For further information, please visit the company website at www.stratamagnetic.com or write the authors at stratamagnetic.software@outlook.com. This work was internally supported by Stratamagnetic Software, LLC. The authors affirm that no competing interests exist.

References

1. Chin, J.A. 2022. "Non-Newtonian Flow in Clogged Non-Circular Piping Conduits." AADE-22-FTCE-006, AADE Fluids Technical Conference and Exhibition, Houston, April 19-20, 2022. Available from www.aade.org.

2. Chin, J.A. and Chin, W.C. 2022. "Non-Newtonian Flow in Bifurcated Piping and Arterial Networks." Special Issue on Multi-Phase Flow With and Without Heat Transfer, Journal of Energy and Power Technology, Volume 4, Issue 1, 2022.